Optical phase diagram of perovskite colossal magnetoresistance manganites near half doping

István Kézsmárki, Y. Tomioka, S. Miyasaka, L. Demkó, Y. Okimoto, Y. Tokura

Optical phase diagram of perovskite colossal magnetoresistance manganites near half doping

I. Kézsmárki,[1,2,3] Y. Tomioka,[4] S. Miyasaka,[1] L. Demkó,[3] Y. Okimoto,[4,5] and Y. Tokura[1,2,4]

[1]*Department of Applied Physics, University of Tokyo, Tokyo 113-8656, Japan*

[2]*Multiferroics Project, ERATO, Japan Science and Technology Agency (JST), Tsukuba 305-8562, Japan*

[3]*Department of Physics, Budapest University of Technology and Economics and Condensed Matter Research Group of the Hungarian Academy of Sciences, 1111 Budapest, Hungary*

[4]*Correlated Electron Research Center (CERC), National Institute of Advanced Industrial Science and Technology (AIST), Tsukuba 305-8562, Japan*

[5]*Department of Materials Science, Tokyo Institute of Technology, Meguro-ku, Tokyo 152-8551, Japan*

We present a systematic optical study for a bandwidth-controlled series of nearly half-doped colossal magnetoresistive manganites $RE_{0.55}AE_{0.45}MnO_3$ (RE and AE being rare earth and alkaline earth ions, respectively) under the presence of quenched disorder over a broad temperature region $T = 10 - 800$ K. The ground state of the compounds ranges from the charge and orbital ordered insulator through the spin glass to the ferromagnetic metal. The enhanced phase fluctuations, namely, the short-range charge and orbital correlations, dominate the paramagnetic region of the phase diagram above all the ground-state phases. This paramagnetic region is characterized by a full-gap to pseudogap crossover toward elevated temperatures where a broad low-energy electronic structure appears in the conductivity spectra over a large variation of the bandwidth. This pseudogap state with local correlations is robust against thermal fluctuations at least up to $T = 800$ K. For a small bandwidth, the onset of the long-range charge order is accompanied by an instantaneous increase of the gap. The emergence of the ferromagnetic state is manifested in the optical spectra as a first-order insulator to a metal transition for compounds with a moderate bandwidth, while it becomes a second-order transition on the larger bandwidth side. An unusually large scattering rate of the metallic carriers is observed in the ferromagnetic state, which is attributed to orbital correlation effects.

PACS number(s): 71.30.+h, 71.27.+a, 78.20.−e

I. INTRODUCTION

The accumulation of dopant charges in Mott insulators and the dependence of the critical doping level on the relative strength of the Coulomb repulsion have been studied for a large variety of correlated electron systems.[1–3] Generally, with increasing U/W ratio (where U is the onsite Coulomb interaction and W the effective one-electron bandwidth), the insulating phase becomes more robust against doping-induced insulator to metal transition.

In perovskite-type manganites, due to the strong interplay between electronic charge, spin, orbital, and lattice degrees of freedom, at specific carrier concentrations (so-called commensurate doping levels) several charge and orbital ordered (CO/OO) patterns emerge, accompanied by antiferromagnetic ordering.[4,5] These CO/OO states are inherently insulator types, and in their vicinity charge and orbital correlation effects are critically intensified. Consequently, for the compounds with relatively narrow one-electron bandwidths the CO/OO ground state remains stable against considerable variation of doping and hence the metallic conduction does not appear.[6–8] However, at a fixed carrier concentration, as the bandwidth of the e_g electrons is increased, the CO/OO suddenly collapses and the compound goes through a first-order insulator to metal transition and simultaneously an antiferromagnetic to ferromagnetic transition.[7,8] This tendency is discerned in Fig. 1(a) in the bandwidth-temperature phase diagram typical of $RE_{1-x}AE_xMnO_3$ (RE and AE being rare earth and alkaline earth ions, respectively) materials close to half doping, namely, for $x = 0.45$ in the present case.

Throughout the paper, we shall refer to the averaged radius of $RE_{1-x}AE_x$ as a measure of the e_g one-electron bandwidth in the sense that it reflects the magnitude of the double exchange interaction responsible for the ferromagnetic (FM) metallic phase.[9] The competition of spin-orbital exchange interaction energies, further balanced by a strong coupling to the lattice, is clearly manifested in the first-order nature of the transition between the two robust phases with ordering temperatures (T_{CO} and T_c, respectively) higher than $T = 200$ K. The first-order transition line separating the two ordered phases is terminated by a bicritical point at as high a temperature as $T_{bicr} \approx 200$ K, indicating the stability of both phases against thermal fluctuations. In contrast, the application of magnetic fields of a few tesla efficiently induces the CO/OO AFI to FM transition, implying the precise balance of the free energy for the two neighboring ground states.[6,7,10,11] These result in gigantic phase fluctuations above the bicritical point and cause the onset of the ordered phase with decreasing temperature to also occur in a first-order-transition manner on either side of the bicritical point.[8,12–14] Among macroscopic quantities, colossal magnetoresistance (CMR) is the most dramatic manifestation of this phase-fluctuation-induced phenomenon.[15,16]

In perovskite-type manganites, the carriers are doped via the partial substitution of the RE component with divalent ions in the form of $RE_{1-x}AE_xMnO_3$, where AE=Ca, Sr, and Bausnally. In addition to the change of the band filling, this random doping introduces quenched disorder into the lattice, which can result in a critical suppression of the long-range order on both sides of the bicritical point [Fig. 1(b)]. The variance of the ionic radius at the perovskite A site was
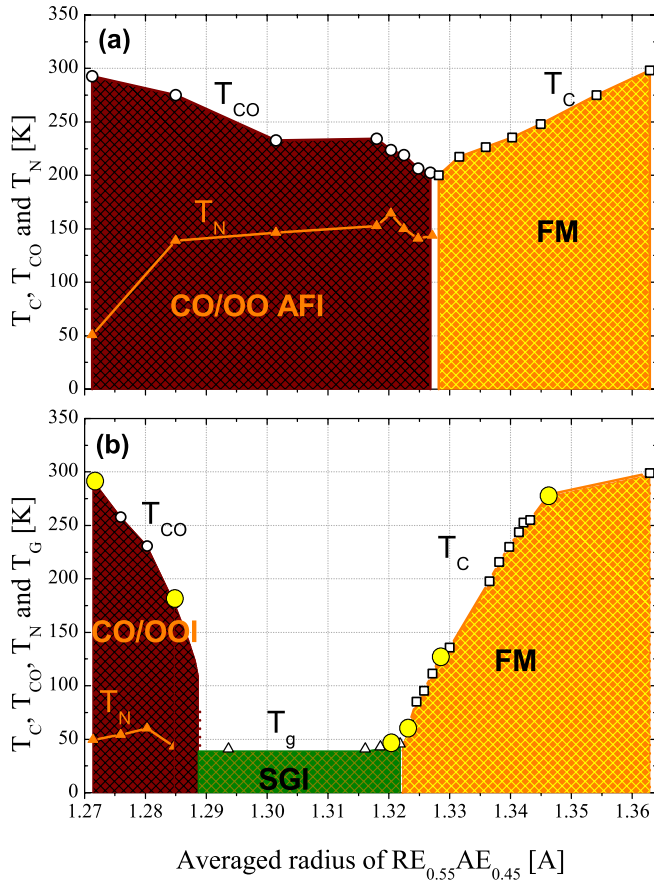
FIG. 1. (Color online) Bandwidth-temperature phase diagram of colossal magnetoresistance manganites near-half doping with low and high levels of quenched disorder displayed in the upper and lower panels, respectively [reproduced from Tomioka and Tokura (Ref. 8)]. In panel (a), T_{CO} and T_C meet at ~ 200 K and form the so-called bicritical point, while in panel (b), the ordered phases are suppressed and an intermediate spin glass phase appears below T_g due to the quenched disorder. The compounds investigated in the present optical study are highlighted in panel (b).

found to well represent the degree of disorder.[17,18] For the compounds in Fig. 1(a), the variance is rather low, while it is considerably large for those in Fig. 1(b). Therefore, they will be referred to as low- and high-disorder phase diagrams, respectively.

The long-range CO/OO AFI state is primarily sensitive to the local lattice distortion and loses territory toward a larger variance. The broad intermediate region bounded by the two ordered phases in Fig. 1(b) is characterized by short-range CO/OO correlation enhanced toward low temperatures and finally frozen to an insulating glassy state (SGI) below T_g. The weakening of the ferromagnetism or the critical suppression of T_c close to the bicritical point is probably the result of CO/OO fluctuations as well. This was indeed observed in recent x-ray diffuse scattering and Raman scattering experiments: Similar to the temperature region above T_{CO} and T_g,[19–21] for a larger bandwidth, the CO/OO correlation is also critically enhanced toward low temperatures where it was suddenly cut by the first-order FM transition.[22] Therefore, it seems very plausible to consider that the paramagnetic re-

gion above all the ground-state phases is essentially governed by a strong short-range correlation of the CO/OO phase in addition to FM spin fluctuations.[23]

In an effort to understand the details of the CMR effect for nearly half-doped perovskite manganites with high quenched disorder—beyond the basic picture capturing the role of competing magnetic exchange interactions and interlocking of spin, charge, orbital, and lattice degrees of freedom[24,25]—several intrinsic and extrinsic mechanisms have been proposed. The former treats CMR as a result of strong fluctuations of a homogeneous quantum phase,[11,12,21] while the latter considers disoder-induced phase separation and percolation effects indispensable for the description of the phenomenon.[26–28] Recently, the existence of topological defects in the orbital order, namely, orbital solitons carrying $\pm e/2$ charge, for manganites close to half doping were also suggested as a natural explanation of nanoscale inhomogeneities in these materials.[29]

In order to investigate the influence of the dramatic phase change and enhanced CO/OO fluctuations on the low-energy electronic states of CMR manganites, we performed a systematic optical study over the compounds highlighted in Fig. 1(b). Changing the chemical composition along this series results dominantly in a variation of the bandwidth, while the level of quenched disorder is kept relatively high. The presence of neighboring phases with different types of orbital order in nearly half-doped perovskite manganites[15,30–32] also gives the hint that a critical amplification of orbital fluctuations may play a unique role in CMR effect. The main goal of the paper is to follow the fingerprints of short-range CO/OO correlation in the low-energy optical conductivity spectra of $RE_{0.55}AE_{0.45}MnO_3$ compounds over a broad range of the bandwidth-temperature phase diagram. The systematics of the low-energy electronic structure, obtained in the course of the present optical study and discussed in the body of the paper, are visualized in Fig. 2.

II. EXPERIMENTAL DETAILS

All of the $RE_{0.55}AE_{0.45}MnO_3$ samples (RE=Nd, Sm, Eu, and Gd; AE=Ca and Sr) investigated here were single crystals grown by a floating-zone method.[22] Throughout the paper, for $Nd_{0.55}Sr_{0.45}MnO_3$, $Sm_{0.55}Sr_{0.45}MnO_3$, $Eu_{0.55}Sr_{0.45}MnO_3$, $Gd_{0.55}Sr_{0.45}MnO_3$, $Gd_{0.55}(Ca_{0.75}Sr_{0.25})_{0.45}MnO_3$, and $Gd_{0.55}Ca_{0.45}MnO_3$, we use the abbreviations NSMO, SSMO, ESMO, GSMO, GCSMO, and GCMO, respectively. In the CO/OO state, these compounds are characterized by electron dynamics with a nearly isotropic optical conductivity within the *ab* plane and with reduced low-energy spectral weight for polarization along the *c* axis.[31] Therefore, in the present systematic study of the optical properties over a broad range of the bandwidth-temperature plane, we used oriented single crystals and measured reflectivity spectra at nearly normal incidence on the (001) crystallographic plane (in the pseudocubic setting). The samples were cut and polished with alumina powder to the optical flatness. In order to eliminate residual strains of surface layers induced by mechanical polishing, the crystals were annealed at 1300 °C for about 30 h.[33]
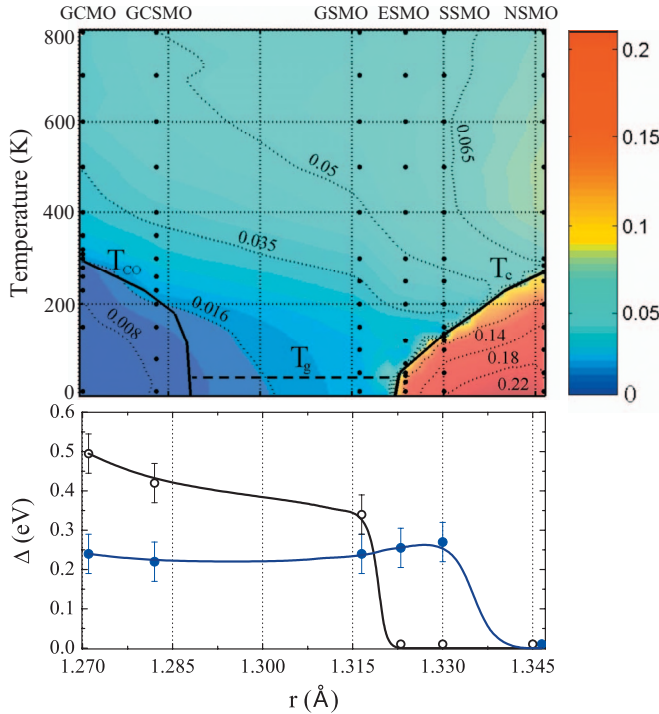
FIG. 2. (Color) Optical phase diagram of nearly half-doped RE$_{0.55}$AE$_{0.45}$MnO$_3$ CMR manganites. Upper panel: Contour map for the low-energy spectral weight, i.e., $N_{eff}(\omega=0.68$ eV$)$, over the average ionic radius (r) vs temperature plane. The abbreviations for the name of the compounds are introduced in Sec. II. The map is obtained by the interpolation of the experimental data indicated by black dots. Besides the color scaling, numerical values are also given on the contour lines for reference. Phase boundaries are also indicated by showing the CO/OO, SGI, and FM transition temperatures. Lower panel: Variation of the charge gap Δ with the ionic radius (equivalent to the effective one-electron bandwidth). The ground-state ($T=10$ K) gap is plotted by open circles. For comparison, the gap value just above T_{CO} (GCMO, GCSMO) and T_c (ESMO, SSMO, and NSMO) and at $T=200$ K for GSMO, shown by full symbols. The solid lines are merely a guide to the eyes.

Reflectivity spectra were investigated in a photon-energy range of $E=3$ meV–6 eV below room temperature and in a slightly limited range ($E \geq 80$ meV) for $T=10$–800 K. For the proper Kramers-Kronig analysis, the room temperature measurements were extended up to 40 eV with the use of synchrotron radiation at UV-SOR, Institute for Molecular Science at Okazaki. Although the obtained conductivity spectra cover the whole range of representative charge-transfer excitations,[34] we focus here on the low-energy part governed by correlation effects. In our convention, $\sigma(\omega)$ denotes the real part of the optical conductivity simply referred to as the optical conductivity.

III. EVOLUTION OF THE GROUND STATE

The temperature dependence of the dc resistivity measured on the respective single crystals by the standard four-probe method is shown in Fig. 3. The onset of the CO/OO or the FM transition is clearly manifested in the resistivity
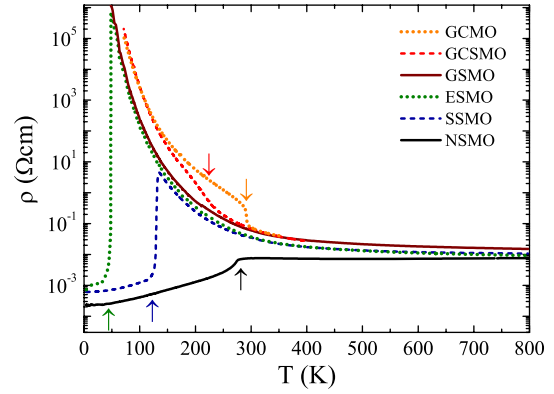

FIG. 3. (Color online) Temperature dependence of the resistivity for RE$_{0.55}$AE$_{0.45}$MnO$_3$ single crystals (RE=Nd, Sm, Eu, and Gd; AE=Ca and Sr). The arrows indicate the first-order transition to the ferromagnetic ground state for NSMO, SSMO, and ESMO and the onset of the charge ordered state in GCSMO and GCMO.

curves, as indicated by arrows. As a general tendency, with increasing bandwidth, T_{CO} steeply decreases. In the case of Gd$_{0.55}$Sr$_{0.45}$MnO$_3$ with the glassy ground state, although the long-range CO/OO order is lost, the system remains insulating. Upon further increase of the bandwidth, the low-temperature phase becomes a ferromagnetic metal, as discerned in Fig. 3 for R=Eu, Sm, and Nd. The dc conductivity ($\sigma_{dc} \equiv 1/\rho$) shows an overall agreement with the value obtained by the zero-energy extrapolation of the optical conductivity spectra for each metal. The difference, a factor of ~3 for R=Eu and Sm, is likely due to localization effects, which may have a major influence on the dc transport and lowest-energy optical conductivity but does not remarkably affect the optical conductivity spectra in the energy region covered by the present study. Irrespective of the ground-state nature, the $\rho(T)$ curves tend to converge in the high-temperature disordered phase. In fact, the difference at room temperature is only 1 order of magnitude, and it is further reduced down to a factor of ~2 at the elevated temperature, $T=800$ K. This tendency will be discussed in the context of the optical conductivity spectra.

For the study of the bandwidth-controlled low-energy spectral changes, we mostly focus on the intraband transitions of the Mn 3d electrons (hybridized with O 2p states) located below ~2 eV. The ground-state conductivity spectra for the two end compounds are plotted over a broader energy range up to ~4.5 eV in the inset of Fig. 4. Gd$_{0.55}$Ca$_{0.45}$MnO$_3$ is an insulator with a charge gap $\Delta_{cg} \approx 0.5$ eV. The broad peak located at around $E_{peak}=1.4$ eV corresponds to optical transition of $d_{3x^2-r^2}$ and $d_{3y^2-r^2}$ electrons to the neighboring Mn^{4+} site with a parallel spin and therefore related to the intersite Coulomb interaction. It is separated by a clear minimum from the higher-lying Mn 3$d \rightarrow$ O 2p charge-transfer excitations centered at ~4 eV. On the other hand, Nd$_{0.55}$Sr$_{0.45}$MnO$_3$ shows a metalliclike optical response. Parallel to the enhanced low-energy spectral weight, the oscillatory strength of the charge-transfer peak is reduced, indicating a stronger hybridization between Mn 3d and O 2p electrons, as expected within the framework of a double exchange mechanism.
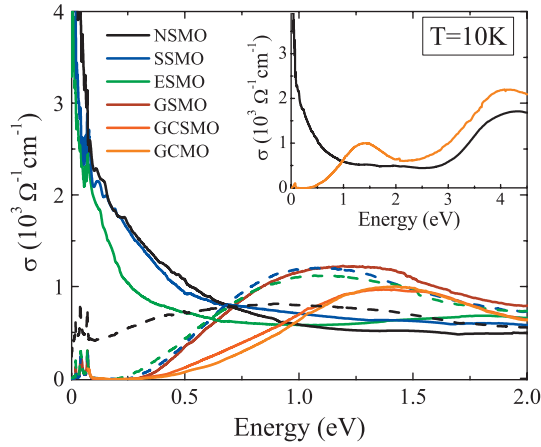
FIG. 4. (Color) Comparison of the ground-state optical conductivity spectra for a bandwidth-tuned series of $RE_{0.55}AE_{0.45}MnO_3$ manganites (full lines). The dashed lines correspond to optical conductivity of NSMO, SSMO, and ESMO in their most insulating state, i.e., just above T_c. The inset shows the conductivity spectra of the two end compounds on a wider energy scale.

The evolution of the low-energy optical conductivity spectra with the variation of the bandwidth is discerned in Fig. 4. Three distinct spectral shapes are observed: (i) The two CO/OO compounds have a charge gap $\Delta_{cg} \approx 0.5$ eV followed by a broad peak at $E_{peak} = 1.4$ eV. (ii) In the case of $Gd_{0.55}Sr_{0.45}MnO_3$ with the glassy ground state, the presence of the charge gap is still clear although it is smaller in magnitude and the E_{peak} is simultaneously reduced. (iii) The three FM compounds exhibit broad metallic conductivity spectra with strong incoherent, i.e., only gently w-dependent, character up to ~ 0.5 eV, which is typical of CMR manganites. Since the spin sector is fully polarized at low temperatures, orbital fluctuations are likely responsible for the enhanced scattering amplitude. Besides the ground-state spectra, the optical conductivity just above T_c is also plotted for the FM compounds. Except for $Nd_{0.55}Sr_{0.45}MnO_3$ with the largest bandwidth, they resemble that of $Gd_{0.55}Sr_{0.45}MnO_3$ in its glassy ground state; the charge gap characteristic of the short-range CO/OO phase is already developed at elevated temperatures above the onset of the ferromagnetic metallic state. We just note here and discuss later in detail that the gap of the two CO/OO materials shows a discontinuous decrease at T_{CO} and that just above the CO/OO transition, it is also close to the ground-state value of $Gd_{0.55}Sr_{0.45}MnO_3$.

IV. CROSSOVER TOWARD THE HIGH-TEMPERATURE PHASE

Here, we turn to the analysis of the temperature-induced spectral-weight transfer both for the insulating and metallic compounds. While the charge gap in the CO/OO state of GCMO and GCSMO shows only a weak temperature dependence up to T_{CO}, the loss of the long-range order results in a sudden decrease of the gap energy, as shown in Fig. 5. The shape of their optical conductivity spectra just above the transition resemble that of GSMO in the ground state. Above T_{CO}, the gap is gradually filled by thermal fluctuations, and a

fully incoherent low-energy conductivity emerges. In both compounds, the spectral weight is transferred dramatically through an equal-absorption (isosbestic) point at $\omega_{iso} \approx 1$ eV. Such an equal-absorption point often appears in the optical conductivity spectrum of correlated electron systems and signals the redistribution of the spectral weight between two characteristic energy scales,[35] in the present case, between the in-gap states (with incoherent low-energy conductivity or coherent metallic contribution for larger bandwidth) and $E_{peak} = 1.4$ eV. On the other hand, in GSMO the closing of the gap occurs in a smooth way. Although in either of the three insulators the metallic conductivity is not fully recovered at any temperature, the development of an incoherent contribution to the optical conductivity implies the partial liberation of the orbital degrees of freedom in the e_g sector. More specifically, the reduced gap in the glassy ground state of GSMO and above T_{CO} in the CO/OO insulators is due to orbital redistribution of the excess electrons (5% relative to the $x = 1/2$ commensurate level), which occupy $d_{3z^2 - r^2}$ orbitals of originally Mn^{4+} sites in the long-range ordered state.[5] Their optical transitions dominating the c-axis conductivity are characterized by a remarkably smaller gap energy as observed in $Pr_{0.6}Ca_{0.4}MnO_3$.[6] The melting of this CO/OO phase means the emergence of a charge-orbital liquid state in which the local CO/OO correlations are still dominant and, together with a dynamical Jahn-Teller effect, preserve electron localization. Toward high temperatures, the electronic state of the three insulators becomes similar, as manifested in their nearly identical optical conductivity spectra above $T = 600$ K.

At the metallic side of the phase diagram, the gradual transfer of the low-energy spectral weight to the ~ 1 eV peak occurs when T_c is approached (see Fig. 6). In this case the isosbestic behavior is also discerned with an equal-absorption point at $\omega_{iso} \approx 0.68$ eV. Its energy scale is considerably lower than in the CO/OO insulators but close to that of GSMO. The ferromagnetic to paramagnetic transition is associated with a dramatic redistribution of the spectral weight, especially in ESMO and SSMO where the instantaneous opening of the charge gap is observed above T_c. In NSMO with a larger bandwidth (and equivalently with a higher Curie temperature), the transition occurs in a continuous manner and only a pseudogap develops in the paramagnetic (PM) phase. The change in the character of the FM transition (from first to second order) between SSMO and NSMO can be well followed in the lower panel of Fig. 2 as well, where the charge gap is plotted for the whole series of the compounds both along the $T_{CO}(r, T)$ and $T_c(r, T)$ phase boundaries. With increasing bandwidth, the gap evaluated at the lowest temperature of the PM phase shows only a tiny variation around $\Delta = 0.25$ eV until SSMO while it completely vanishes for NSMO. Detailed magnetotransport and magnetization studies also reveal that the first-order PM-FM phase boundary is terminated between SSMO and NSMO, and the transition becomes continuous for larger bandwidths.[36] The presence of first-order phase boundaries (indicated by a thick line in both panels of Fig. 1) separating the FM state both from the CO/OO and PM phase implies dramatic change in the orbital character of e_g electrons. Although it is a central issue in the CMR physics, the orbital nature of the FM state
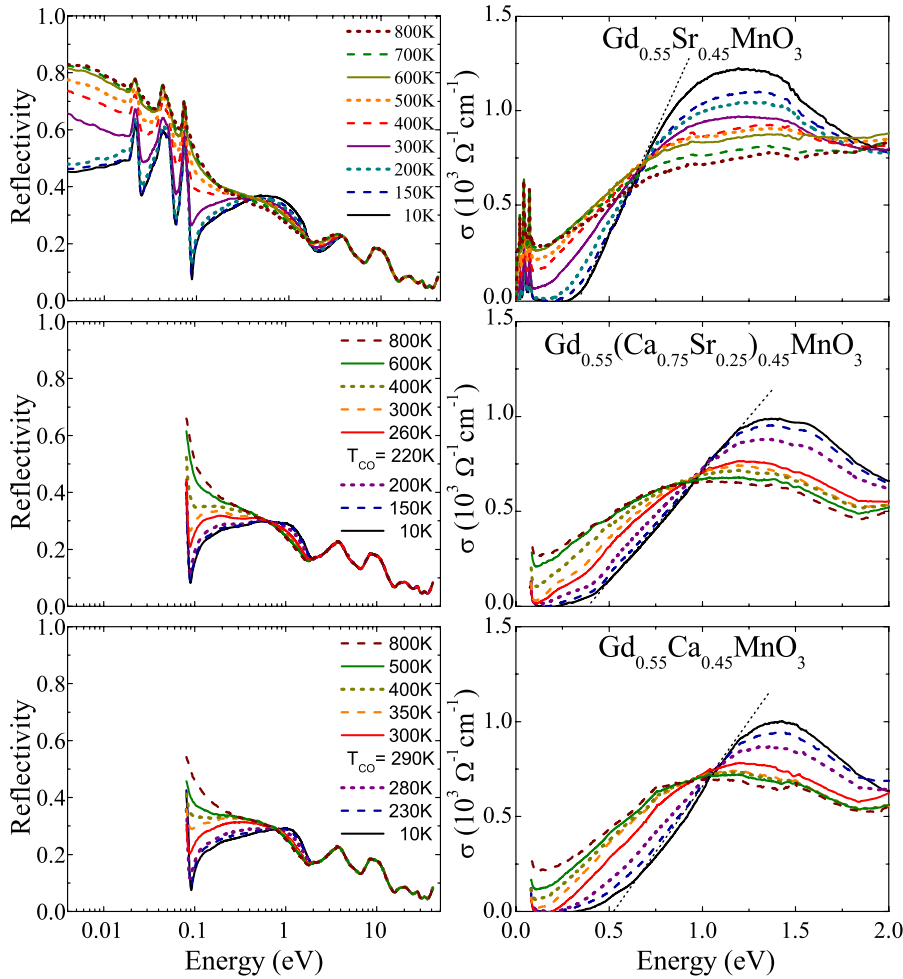
FIG. 5. (Color online) Reflectivity and conductivity spectra of the three insulators GCMO, GCSMO, and GSMO at selected temperatures (left and right panel, respectively). Note the difference in energy scales in the left (logarithmic) and right (linear) panels. The linear extrapolation to estimate the gap energy in the ground state is shown by black dotted lines. The temperature of the CO/OO transition is indicated in the label.

has not utterly been clarified. In the present optical study, the question is also to address in the context of the large scattering rate observed in the fully spin-polarized low-temperature state. For the present metals, three possible scenarios have been proposed: (i) a disordered phase involving both ($x^2 - y^2$) and ($3z^2 - r^2$) orbitals[31] or strong ferro-orbital correlations of either (ii) the planar ($x^2 - y^2$) type[37,38] or (iii) the rodlike ($3z^2 - r^2$) type.[32] In the case of SSMO, the development of a rodlike order is supported by recent neutron scattering experiments; the anomalously large fourth-neighbor interaction along the x (or y or z) direction, $J_4 \approx 0.6J_1$, implies the extended one-dimensional exchange path reflecting the rodlike orbital correlation.[32] The effect of the orthorhombic lattice distortion is almost negligible for SSMO (which is also the case for ESMO and NSMO); the spatial and temporal fluctuations of the nearly equivalent [001], [010], and [100] domains may prevent the onset of a static long-range orbital ordering for the investigated temperature region. The optical isotropy of the ab plane also implies the lack of long-range order above $T = 10$ K; thus, the robust enhancement of the metallic conductivity in the vicinity of the ferromagnetic transition is attributable to the instantaneous onset of the spin polarization below T_c. Thus, the large scattering rate preserved within the spin-polarized phase implies the essential role of orbital fluctuations in the charge dynamics. The results are consistent with the rodlike orbital order; however, it

does not contradict the other two scenarios either.

At room temperature, which is slightly above both the FM and CO/OO phases, the optical conductivity spectra of the respective materials are close to each other, irrespective of the nature of the ground state. Similar to the tendency observed for the resistivity curves, they further converge and become nearly identical at the highest temperature of the present optical study, $T = 800$ K, as discerned in Fig. 7. A systematic analysis of the low-energy spectral changes is given in Fig. 8 where the temperature dependence of the spectral weight, i.e., the effective number of electrons defined as $N_{eff}(\omega_c) = 2m_0(\pi e^2 N)^{-1} \int_0^{\omega_c} \sigma(\omega) d\omega$, for $\omega_c = 0.1$ and 0.68 eV is simultaneously plotted for each compound. The former solely represents the metallic conductivity, while the latter corresponds to the energy scale of the equal-absorption point, therefore including the strong incoherent midinfrared contribution. Except for the FM phase where a stronger enhancement due to the development of coherent conduction is found in $N_{eff}(\omega_c = 0.1$ eV), the temperature dependence of the spectral weight is rather similar for both energy scales. This implies that the low-energy excitations, i.e., the in-gap states, are fully governed by CO/OO correlations.

The variation of the total spectral weight, represented by $N_{eff}(\omega_c = 0.68$ eV), is also visualized over the whole phase diagram in the color contour plot of Fig. 2. Both the dramatic increase in N_{eff} below T_c and its reduction below T_{CO} are
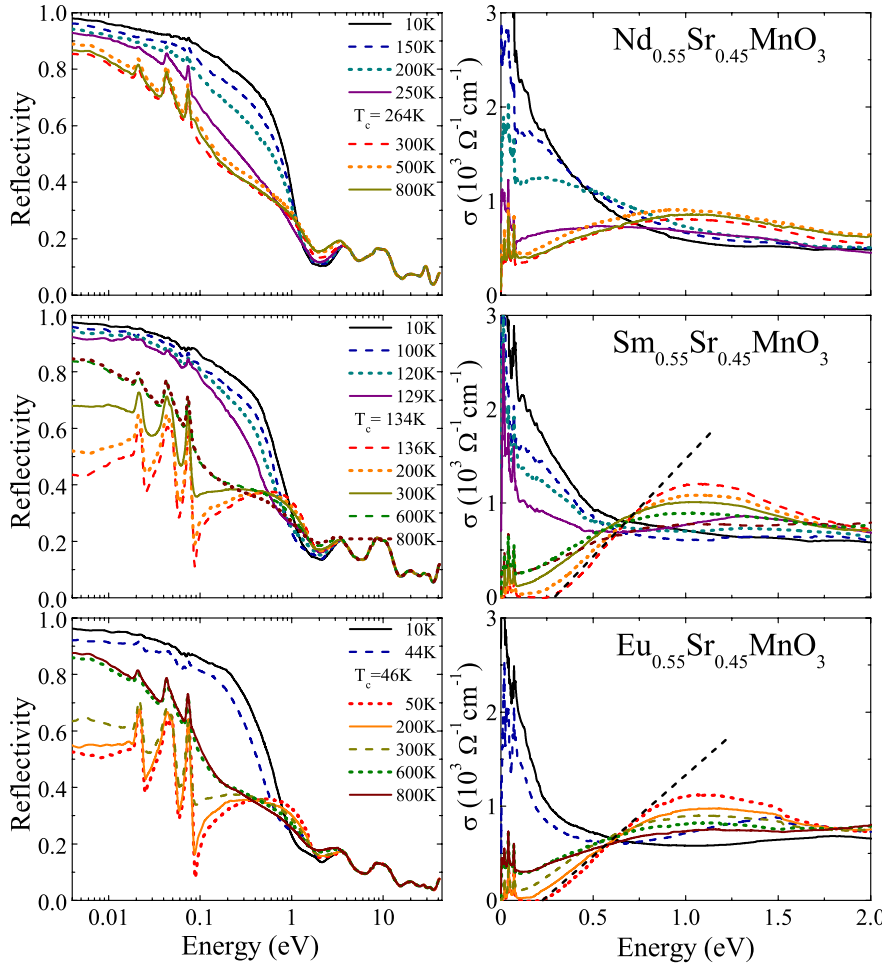
FIG. 6. (Color online) Reflectivity and conductivity spectra of the three metals ESMO, SSMO, and NSMO at selected temperatures (left and right panel, respectively). For ESMO and SSMO, the linear extrapolation to estimate the gap energy just above the FM transition is shown by dotted lines.

clearly manifested in the contour plot. The light-blue region of the phase diagram characterized by a flat low-energy conductivity spectrum demonstrates the strong CO/OO fluctuations extending above all the three underlying phases. The pseudogaplike feature of the optical spectra (i.e., the presence of the midinfrared peak and the reduced optical weight below it) is preserved, and the metallic conductivity is not recovered up to $T=800$ K, indicating the subsisting CO/OO correlations up to higher temperatures in this critically doped series of CMR manganites. On the other hand, x-ray experiments on the same materials could detect the diffuse scattering arising from the short-range orbital ordering, but no longer than up to $T=400$ K.[22] This means that above this temperature, the correlation length of the lattice distortion is limited to the scale of the unit cell. However, infrared optical excitations can still sensitively pick up the local orbital configuration and thus give a direct tool for charge-orbital correlation effects in these materials. This scenario is in full agreement with the results of recent neutron scattering experiments performed on the series of $La_{1-x}Ca_xMnO_3$, with $x=0-0.5$.[39] These structural studies reveal that the local Jahn-Teller distortion is present over the whole insulating phase, namely, for each concentration and up to at least $T=500$ K. Furthermore, in the paramagnetic phase above the FM ground state, the range of the Jahn-Teller distortion is found to be restricted to single MnO_6 octahedra.[40]
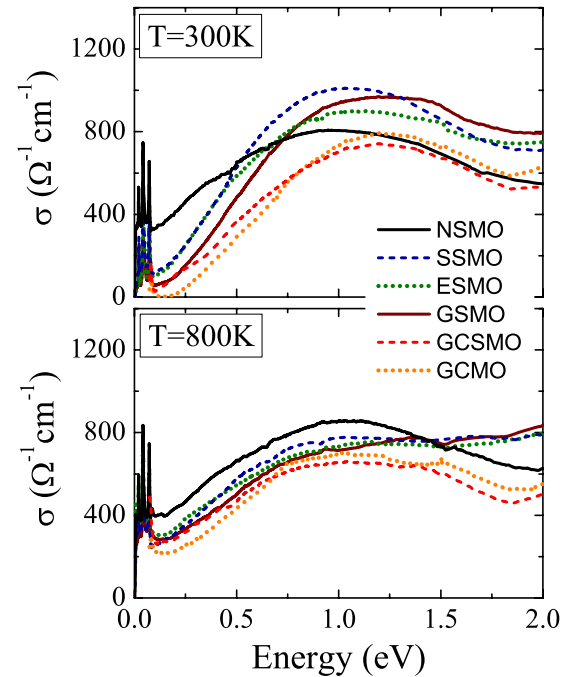

FIG. 7. (Color online) Comparative plot of the optical conductivity for the full series of $RE_{0.55}AE_{0.45}MnO_3$ manganites at $T=300$ and 800 K (upper and lower panels, respectively).
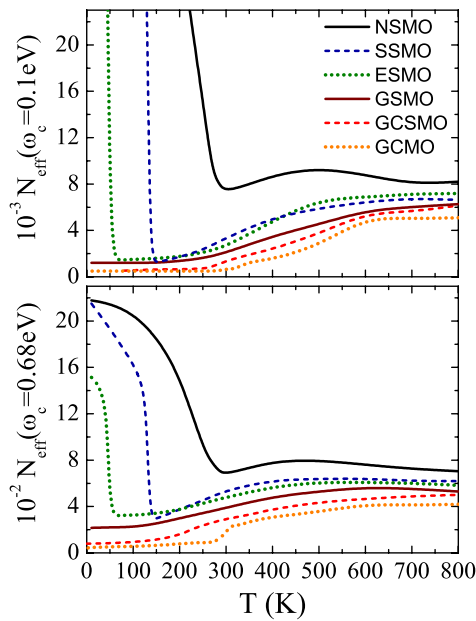
FIG. 8. (Color online) Temperature dependence of the effective number of electrons, $N_{eff}(\omega_c)$, at two representative energies $\omega_c = 0.1$ and 0.68 eV for the bandwidth-tuned series of $RE_{0.55}AE_{0.45}MnO_3$ manganites shown in the upper and lower panels, respectively.

V. CONCLUSIONS

The aim of the present optical study of nearly half-doped colossal magnetoresistive manganites $RE_{0.55}AE_{0.45}MnO_3$ with large quenched disorder was to characterize the nature of the low-energy electronic states responsible for the CMR effect. We have investigated the systematics of the optical conductivity spectrum over a broad area of the bandwidth vs temperature plane. The ground state of the compounds ranges from the charge and orbital ordered insulator through the spin glass to the ferromagnetic metal. The key role of critically enhanced phase fluctuations, most typically the short-range CO/OO correlation, was found in the paramagnetic region of the phase diagram above all the ground-state phases. This charge-orbital liquid state is characterized by a pseudogap below $E_{peak} \approx 1$ eV in the optical conductivity and flat low-energy optical conductivity spectrum over a large variation of the bandwidth. It is robust against thermal agitations and extends up to as high a temperature as $T = 800$ K. The onset of the long-range charge order is accompanied by an instantaneous increase of the gap. The emergence of the ferromagnetic state is manifested in the optical spectra as a first order insulator to metal transition for compounds with a moderate bandwidth, while it becomes a continuous transition on the largest bandwidth side. An unusually large scattering rate of the metallic carriers is observed in the ferromagnetic state, which is attributed to orbital correlation effects.

[1] T. Katsufuji, Y. Okimoto, and Y. Tokura, Phys. Rev. Lett. **75**, 3497 (1995).

[2] Y. Okimoto, T. Katsufuji, Y. Okada, T. Arima, and Y. Tokura, Phys. Rev. B **51**, 9581 (1995).

[3] M. Imada, A. Fujimori, and Y. Tokura, Rev. Mod. Phys. **70**, 1039 (1998).

[4] J. B. Goodenough, Phys. Rev. **100**, 564 (1955).

[5] Z. Jirak, S. Krupicka, Z. Simsa, M. Dlouha, and S. Vratislav, J. Magn. Magn. Mater. **53**, 153 (1985).

[6] Y. Okimoto and Y. Tokura, J. Supercond. **13**, 271 (2000).

[7] Y. Tomioka and Y. Tokura, Phys. Rev. B **66**, 104416 (2002).

[8] Y. Tomioka and Y. Tokura, Phys. Rev. B **70**, 014432 (2004).

[9] N. Furukawa, J. Phys. Soc. Jpn. **64**, 2734 (1995).

[10] Y. Tomioka, H. Hiraka, Y. Endoh, and Y. Tokura, Phys. Rev. B **74**, 104420 (2006).

[11] Y. Tokura and N. Nagaosa, Science **288**, 462 (2000).

[12] S. Murakami and N. Nagaosa, Phys. Rev. Lett. **90**, 197201 (2003).

[13] C. P. Adams, J. W. Lynn, V. N. Smolyaninova, A. Biswas, R. L. Greene, W. Ratcliff, S. W. Cheong, Y. M. Mukovskii, and D. A. Shulyatev, Phys. Rev. B **70**, 134414 (2004).

[14] K. H. Kim, S. Lee, T. W. Noh, and S. W. Cheong, Phys. Rev. Lett. **88**, 167204 (2002).

[15] Y. Tokura, Rep. Prog. Phys. **69**, 797 (2006).

[16] T. V. Ramakrishnan, J. Phys.: Condens. Matter **19**, 125211 (2007).

[17] L. M. Rodriguez-Martinez and J. P. Attfield, Phys. Rev. B **54**, R15622 (1996).

[18] L. M. Rodriguez-Martinez and J. P. Attfield, Phys. Rev. B **63**, 024424 (2000).

[19] S. Shimomura, T. Tonegawa, K. Tajima, N. Wakabayashi, N. Ikeda, T. Shobu, Y. Noda, Y. Tomioka, and Y. Tokura, Phys. Rev. B **62**, 3875 (2000).

[20] Z. Jirak, F. Damay, M. Hervieu, C. Martin, B. Raveau, G. Andre, and F. Bouree, Phys. Rev. B **61**, 1181 (2000).

[21] R. Mathieu, D. Akahoshi, A. Asamitsu, Y. Tomioka, and Y. Tokura, Phys. Rev. Lett. **93**, 227202 (2004).

[22] Y. Tomioka, Y. Okimoto, J. H. Jung, R. Kumai, and Y. Tokura, Phys. Rev. B **68**, 094417 (2003).

[23] Y. Motome, N. Furukawa, and N. Nagaosa, Phys. Rev. Lett. **91**, 167204 (2003).

[24] A. J. Millis, P. B. Littlewood, and B. I. Shraiman, Phys. Rev. Lett. **74**, 5144 (1995).

[25] N. Furukawa, J. Phys. Soc. Jpn. **63**, 3214 (1994).

[26] M. Uehara, S. Mori, C. H. Chen, and S.-W. Cheong, Nature (London) **399**, 560 (1999).

[27] E. Dagotto, *Nanoscale Phase Separation and Colossal Magnetoresistance: The Physics of Manganites and Related Com-*

pounds (Springer-Verlag, New York, 2002).

[28] R. P. Rairigh, G. Singh-Bhalla, S. Tongay, T. Dhakal, A. Biswas, and A. F. Hebard, Nat. Phys. **3**, 551 (2007).

[29] L. Brey and P. B. Littlewood, Phys. Rev. Lett. **95**, 117205 (2005).

[30] Y. Konishi, Z. Fang, M. Izumi, T. Manako, M. Kasai, H. Kuwahara, M. Kawasaki, K. Terakura, and Y. Tokura, J. Phys. Soc. Jpn. **68**, 3790 (1999).

[31] K. Tobe, T. Kimura, and Y. Tokura, Phys. Rev. B **69**, 014407 (2004).

[32] Y. Endoh, H. Hiraka, Y. Tomioka, Y. Tokura, N. Nagaosa, and T. Fujiwara, Phys. Rev. Lett. **94**, 017206 (2005).

[33] E. Saitoh, Y. Okimoto, Y. Tomioka, T. Katsufuji, and Y. Tokura, Phys. Rev. B **60**, 10362 (1999).

[34] T. Arima and Y. Tokura, J. Phys. Soc. Jpn. **64**, 2488 (1995).

[35] M. Eckstein, M. Kollar, and D. Vollhardt, J. Low Temp. Phys. **147**, 279 (2007).

[36] L. Demkó, I. Kézsmárki, G. Mihály, N. Takeshita, Y. Tomioka, and Y. Tokura, arXiv:0711.4296 (unpublished).

[37] G. Khaliullin and R. Kilian, Phys. Rev. B **61**, 3494 (2000).

[38] S. Ishihara, M. Yamanaka, and N. Nagaosa, Phys. Rev. B **56**, 686 (1997).

[39] E. S. Bozin, M. Schmidt, A. J. DeConinck, G. Paglia, J. F. Mitchell, T. Chatterji, P. G. Radaelli, Th. Proffen, and S. J. L. Billinge, Phys. Rev. Lett. **98**, 137203 (2007).

[40] R. Bindu, S. K. Pandey, A. Kumar, S. Khalid, and A. V. Pimpale, J. Phys.: Condens. Matter **17**, 6393 (2005).